CORA Cork Open Research Archive
Cartlann Taighde Oscailte Chorcaí

Title	Tunable quasi-reflectionless bandpass filters using substrate integrated coaxial resonators
Authors	Zhao, Kunchen;Gómez-García, Roberto;Psychogiou, Dimitra
Publication date	2021-07-06
Original Citation	Zhao, K., Gómez-García, R. and Psychogiou, D. (2021) 'Tunable quasi-reflectionless bandpass filters using substrate integrated coaxial resonators', IEEE Transactions on Circuits and Systems II: Express Briefs, 69(2), pp. 379-383. doi: 10.1109/TCSII.2021.3094991
Type of publication	Article (peer-reviewed)
Link to publisher's version	10.1109/TCSII.2021.3094991
Rights	© 2021, IEEE. This work is licensed under a Creative Commons Attribution 4.0 License. For more information, see https://creativecommons.org/licenses/by/4.0/ - https://creativecommons.org/licenses/by/4.0/
Download date	2026-11-17 08:24:25
Item downloaded from	https://hdl.handle.net/10468/11560



University College Cork, Ireland
Coláiste na hOllscoile Corcaigh

Tunable Quasi-Reflectionless Bandpass Filters Using Substrate Integrated Coaxial Resonators

Kunchen Zhao, *Graduate Student Member, IEEE*, Roberto Gómez-García, *Senior Member, IEEE*, and Dimitra Psychogiou, *Senior Member, IEEE*

***Abstract*—This brief reports on the electromagnetic (EM) design and the practical development of frequency-reconfigurable quasi-reflectionless bandpass filters (BPFs) using substrate integrated coaxial (SIC) resonators. The filter concept is based on in-series-cascaded quasi-reflectionless stages that are shaped by a first-order bandpass section and two resistively-terminated first-order bandstop sections. For the first time, we explore the realization of these filters using tunable SIC resonators that exhibit high quality factor (Q) and can be widely tuned with commercially-available linear piezoelectric actuators. Synthesized examples alongside various EM design and practical integration aspects are discussed in detail. The concept is experimentally validated at S-band through the manufacturing and testing of two reconfigurable (one-stage and two-stage) prototypes.**

***Index Terms*—Absorptive filter, coaxial filter, frequency-tunable filter, quasi-reflectionless filter, reflectionless filter.**

I. Introduction

DESPITE in their infancy, reflectionless or absorptive bandpass filters (BPFs) are recently being explored as a compact reflection cancellation mechanism for multi-stage RF front-ends (e.g., in instrumentation systems [1] and in harmonic radars [2]) in which reflected RF signals deteriorate the dynamic range of the overall RF system by creating spurs, standing waves, and unwanted oscillations [3]. Unlike traditional reflective-type BPFs that present a high reactive impedance in their stopband regions, reflectionless BPFs are designed with a 50-Ω impedance for both their passband and stopband ranges. Thus, their direct integration in the RF front-ends of reflection-sensitive systems promises significant size and performance advantages when compared to conventional reflection-cancellation approaches in which bulky ferrite-based circulators (e.g., [4] and [5]) or power-hungry transistor-based non-reciprocal components (e.g., [6]) are employed.

Reflectionless BPFs are typically constructed by adding resistively-terminated bandstop filtering networks at their input ports [7]–[10]. As an example, an input reflectionless tunable BPF with the co-designed function of a power divider is shown in [7]. However, tuning is achieved using trimmer capacitors

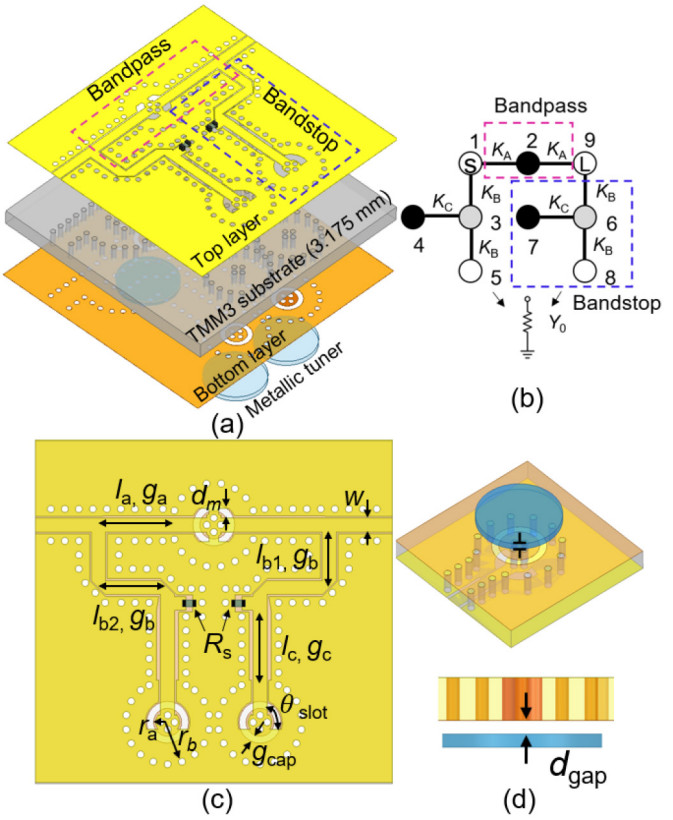


Fig. 1. SIC-resonator-based quasi-reflectionless BPF concept. (a) EM model of the one-stage quasi-reflectionless BPF comprising one bandpass section and two bandstop sections. Frequency tuning is achieved by altering the resonator capacitance through contactless metallic tuners (blue patches). (b) CRD: black circles are resonating nodes, gray circles are non-resonating nodes, and white circles are the source, load, and resistively-terminating nodes. (c) Bottom view showing design parameters. (d) Detail of the tunable SIC resonator. Design parameters are (units in mm): $l_a = 9.84$, $l_{b1} = 6.7$, $l_{b2} = 7.9$, $l_c = 11$, $g_a = 0.28$, $g_b = 0.26$, $g_c = 0.58$, $d_m = 1.4$, $r_a = 2$, $r_b = 6$, $d_{gap} = 1$, and $\theta_{slot} = 80°$; a width of $w = 2$ mm is used in all GCPW TLs and resistive loads $R_s = 50\Omega$ are employed.

Manuscript received March 15, 2021; revised on May 31, 2021; accepted July 3, 2021. Date of publication July 6, 2021; date of current version January 31, 2022. This work was supported in part by the National Science Foundation under Grant ECCS-1731956, and in part by the Spanish Ministry of Economy, Industry, and Competitiveness (State Research Agency) under Project TEC2017-82398-R. This brief was recommended by Associate Editor J. S. Walling. *(Corresponding author: Kunchen Zhao.)*

Kunchen Zhao is with the Department of Electrical, Computer and Energy Engineering, University of Colorado, Boulder, CO 80309 USA (e-mail: kunchen.zhao@colorado.edu).

Roberto Gómez-García is with the Department of Signal Theory and Communications, University of Alcala, 28871 Alcala de Henares, Spain (e-mail: roberto.gomez.garcia@ieee.org).

Dimitra Psychogiou is with the Department of Electrical, Computer, and Energy Engineering, University of Colorado Boulder, Boulder, CO 80309 USA, also with the Department of Electrical and Electronic Engineering, University College Cork, Cork, T12 K8AF Ireland, and also with Tyndall National Institute, Cork, T12 R5CP Ireland (e-mail: dpsychogiou@ucc.ie).

Color versions of one or more figures in this article are available at https://doi.org/10.1109/TCSII.2021.3094991.

Digital Object Identifier 10.1109/TCSII.2021.3094991

This work is licensed under a Creative Commons Attribution 4.0 License. For more information, see https://creativecommons.org/licenses/by/4.0/

that are not electronically tunable. Frequency-tunable reflectionless BPF using lumped-element components [9] or planar microstrip resonators [10] have also been proposed, where the frequency agility is obtained by using surface mount varactors. Despite these configurations being frequency tunable, they are only able to suppress reflections at a single port of the filter. Symmetric reflection-cancellation methods have been demonstrated in [11]–[15]. Nevertheless, most of them rely on specific component element values or use tightly-coupled components, whose characteristics are directly related to the design frequency and the passband bandwidth (BW). As an example, a GaAs-MMIC-based fully-reflectionless BPF is demonstrated in [11] with high selectivity and large rejection ratio. However, it requires unrealistic characteristic impedance values if implemented with transmission-line-based components. In [12], a symmetrical reflectionless BPF is reported with a wide absorptive BW. Nevertheless, it is realized using tightly-coupled gap resonators, which are difficult to be tuned. In addition, all of the aforementioned examples are based on low-quality-factor (Q) lumped element or planar components that result in high in-band insertion loss (IL) (e.g., 3 dB in [11] and 2.4 dB in [13]), limited power-handling capability, and are mostly frequency static.

In order to reduce the IL and maintain a relatively compact volume, substrate-integrated-waveguide-(SIW)-based resonators and filters have been extensively studied as a suitable alternative to traditional planar filter technologies [16], [17]. In particular, substrate-integrated-coaxial-(SIC)-resonator-based filters have been attracting significant interest due to their compact size and the potential for frequency tuning. Although these concepts have been widely explored as reflective BPFs [18]–[21], bandstop filters (BSFs) [22]–[23], and multiband filters [24], yet there is no reported work on SIC-resonator-based reflectionless BPFs.

Considering the aforementioned limitations, this brief reports on the design and practical development of frequency-reconfigurable quasi-reflectionless BPFs using compact SIC resonators. The proposed integration scheme is based on in-series-cascaded stages that exhibit two-port quasi-reflectionless characteristics. The quasi-reflectionless behavior is achieved by adding a bandstop filtering network with a 50-Ω resistive load at the input/output ports. Frequency agility is added by altering the capacitance of the SICs using commercially-available piezoelectric linear actuators. The proposed concept is validated through the manufacturing and testing of a one-stage and a two-stage prototypes.

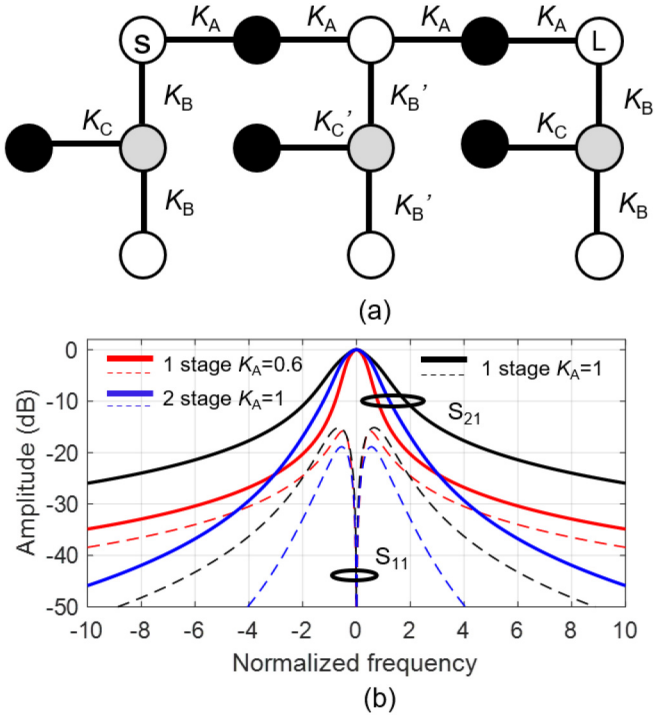


Fig. 2. (a) Normalized CRD of the two-stage quasi-reflectionless BPF. (b) Synthesized power transmission (S_{21}) and reflection (S_{11}) responses of the one- and two-stage BPFs.

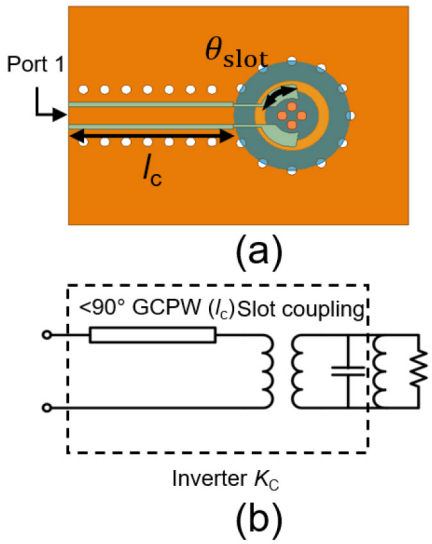


Fig. 3. Detail of the bandstop section that comprises a slot-coupled SIC resonator and a GCPW TL. (a) EM model. (b) Circuit equivalent that consists of an LC tank, and a TL followed by a transformer representing the K_C inverter.

II. Theoretical Foundations

A. Filter Concept and Operating Principles

The details of the quasi-reflectionless SIC-resonator-based BPF concept are shown in Fig. 1 through the conceptual 3D drawing (and EM simulation model) of a single-stage configuration and its corresponding normalized coupling routing diagram (CRD). It is based on three sections, namely a bandpass section that comprises one resonator (resonant node 2) and two inverters K_A, and two resistively-terminated bandstop sections that each consists of one resonator (resonant node 4 or 7) and three inverters K_B and K_C. For the symmetric quasi-reflectionless BPF response to be obtained, the transfer functions of the bandpass and the bandstop sections need to be complementary and fulfill $K_C^2 = K_A^2 \cdot K_B^2$ [12], provided that all resonators are synchronously tuned at the normalized frequency $\Omega = 0$.

An example of synthesized power transmission and reflection responses of the normalized CRD in Fig. 1(b) is illustrated in Fig. 2(b) for the case of $K_A = 1$, $K_B = 1$, and $K_C = 1$, which results in quasi-reflectionless symmetric characteristics with < -15 dB of input reflection across the entire

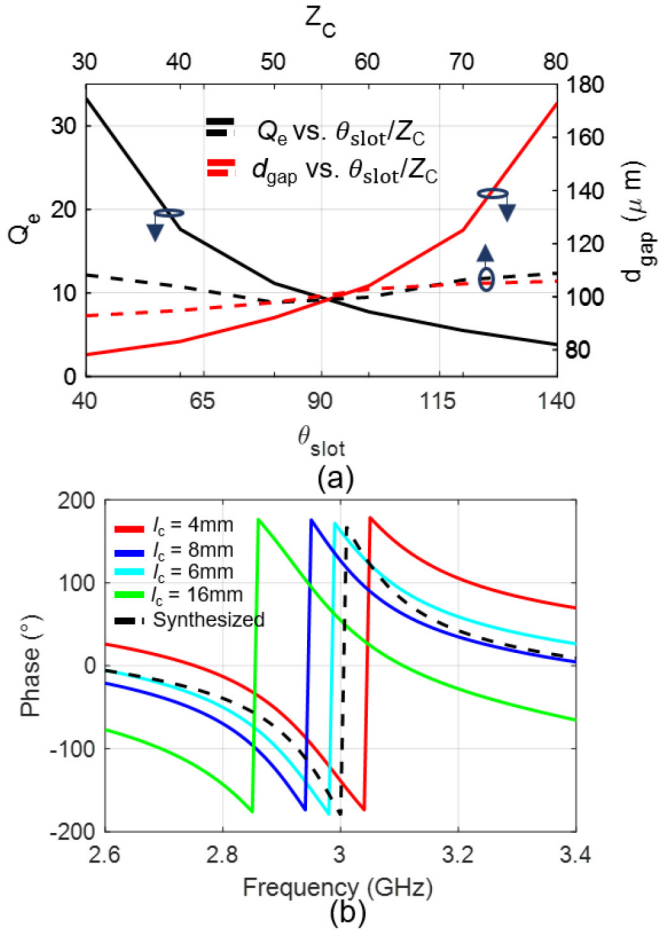


Fig. 4. (a) Simulated Q_e and d_{gap} as a function of θ_{slot} and Z_C for the SIC resonator frequency to be equal to 3 GHz. Q_e is calculated at port 1 of Fig. 3(a). (b) Phase response of an ideal one-port network that consists of one resonator and an ideal K_C inverter and EM-simulated phase response of the coupled resonator section in Fig. 3(a) for $\theta_{\text{slot}} = 80°$ and different l_c, where $l_c = 16$ cm is 90° long at 3 GHz.

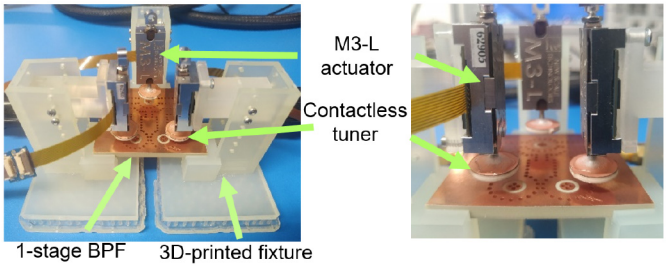


Fig. 5. RF testing setup for the one-stage prototype. A 3D printed fixture was manufactured to assemble the tuners on the BPF.

frequency range. To increase the selectivity and power reflection, multiple replicas of the one-stage configuration can be in-series cascaded, and the overall response of the filter can be calculated as $S_{21}^{N-\text{stage}}(\Omega) = [S_{21}^{\text{one-stage}}]^N$, where N is the number of stages. An example case of a two-stage normalized CRD alongside its corresponding synthesized responses is shown in Fig. 2. It should be noticed that the inverters of the bandstop section that are shared between adjacent stages need to be normalized as $K'_{\text{B}} = \frac{K_{\text{B}}}{\sqrt{2}}$. As also shown in Fig. 2(b), BW control can be obtained by altering K_A.

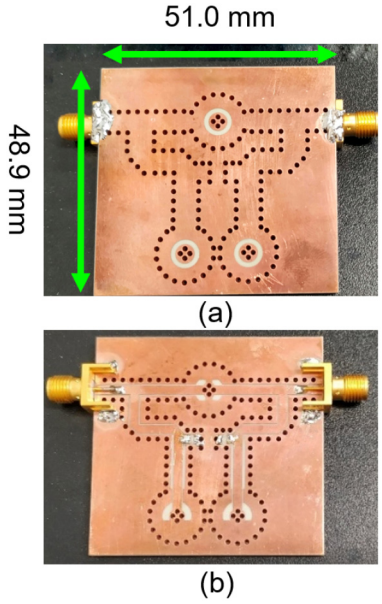


Fig. 6. (a) Front side of the one-stage BPF prototype. (b) Back side of the one-stage BPF prototype.

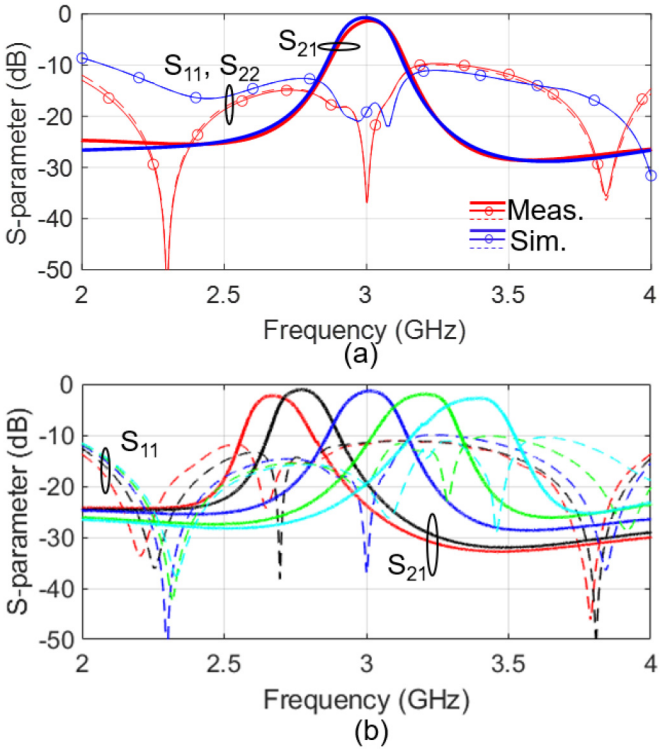


Fig. 7. (a) RF-measured and EM-simulated S-parameters of the one-stage prototype at 3 GHz. (b) RF-measured S-parameters while tuning the capacitively-loaded SIC resonators of the BPF.

B. Practical Design Aspects Using SIC Resonators

To practically realize this filter, a high-Q and compact integration concept using capacitively-loaded SIC resonators and grounded coplanar waveguide (GCPW) transmission-line (TL) inverters is employed as shown in Fig. 1(c). The filter design starts by creating the tunable resonator using the SIC integration scheme in Fig. 1(d), whose fundamental operational

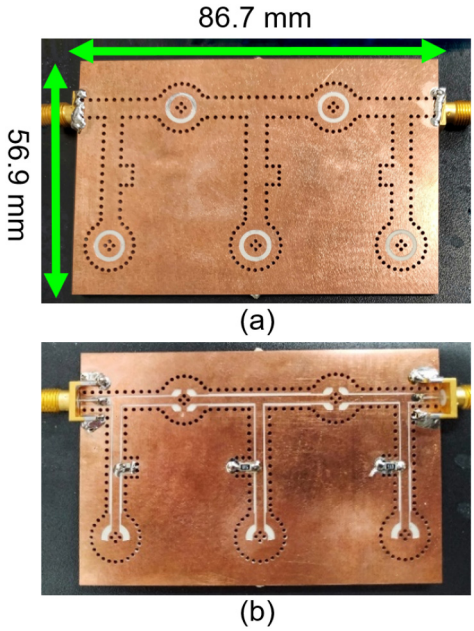


Fig. 8. (a) Front side of the two-stage BPF prototype. (b) Back side of the two-stage BPF prototype.

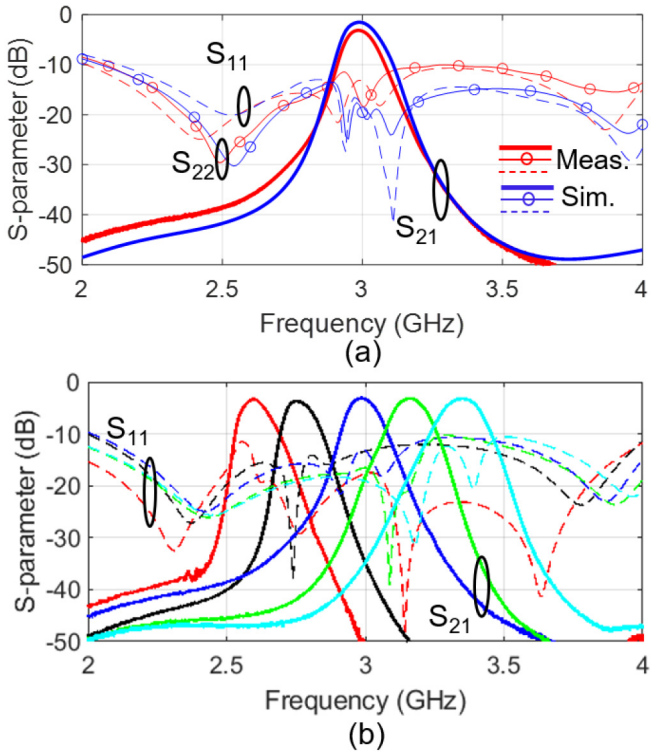


Fig. 9. (a) RF-measured and EM-simulated S-parameters of the two-stage prototype at 3 GHz. (b) RF-measured S-parameters while tuning the capacitively-loaded SIC resonators of the BPF.

principal is discussed in [21]. In particular, the resonator is embedded in a dielectric substrate in which Cu-platted via holes form its cavity walls and the inner conductor of the coaxial. The capacitive loading is materialized by: i) a capacitive ring between the upper end of the inner conductor and the cavity ground (g_{cap}) and ii) a Cu-metalized PCB disk that is positioned on top of the resonator at a distance d_{gap} to the upper cavity wall as shown in Fig. 1(d). Therefore, frequency tuning is achieved by altering d_{gap}, which changes the capacitance of the resonator. The RF signal in each resonator is inserted through slot openings in the bottom ground plane of the filter.

Having designed the tunable SIC resonators, the bandstop and the bandpass sections are designed as follows. In the bandstop section, the K_B inverter between nodes 1 and 3 are implemented with a 90°-long GCPW line with characteristic impedance $Z_{\rm B} = Z_0/K_{\rm B}$ (50 Ω for the case of $K_B = 1$), and the resistively terminated K_B inverter between nodes 3 and 5 loaded with Z_0 is materialized by a single resistor with an equivalent resistance $R_{\rm T} = Z_{\rm B}^2/Z_0$ for size compactness. The detail of the K_C inverter and its equivalent circuit are shown in Fig. 3(a) and (b). It is comprised of two parts, namely a GCPW TL with $Z_{\rm C}$ and length l_C (<90° at f_c) and a slot opening θ_{slot} that couples the RF signal into the SIC resonator. Both of the slot and GCPW TL contribute to the external coupling factor Q_e. (calculated at port 1 in Fig. 3) as shown in Fig. 4. To determinate the value of Z_c and θ_{slot}, for a given $Q_e = 1/(K_{\rm C}^2 \cdot FBW)$ (e.g., for $FBW = 6\%$ and $K_{\rm C} = 1.2$, and $Q_e = 11.5$), EM-simulation-based parametric studies need to be performed. As shown in Fig. 4(a), by increasing $\theta_{\rm slot}$, Q_e decreases. However, this also causes the resonant frequency of the SIC to decrease, which can be counteracted by altering d_{gap}. With Z_C and $\theta_{\rm slot}$ chosen, l_c needs to be defined so that the combined K_C inverter functionalizes the 90° phase inversion at port 1. As shown in Fig. 4(b), a 90°-long TL (defined at 3 GHz) results in an ideal phase inversion at 2.82 GHz, which is lower than the expected 3 GHz. This is attributed to the induced phase shift from the slot opening, which in turn requires l_c to be shortened. It should be noted that l_c does not affect the resonating frequency or Q_e.

III. Experimental Validations

Considering the aforementioned design aspects, a one-stage and a two-stage SIC-based BPFs were designed for a center frequency of 3 GHz and as wide as possible tuning range in the S-band. They were implemented on a Rogers TMM3 substrate (thickness $H = 3.125$ mm, dielectric constant $\epsilon_{\rm r} = 3.32$, loss tangent $\tan\delta = 0.002$, and copper thickness $t = 17\mu$m). The SIC resonator tuner was implemented by a copper-plated circular disk that was attached on the top of a commercially-available digitally-controlled linear actuator from New Scale Tech. [25]. To enable their integration, a multi-part 3D printed fixture was designed and manufactured and is shown in Fig. 5 alongside with the filter assembly during RF testing.

The manufactured one-stage quasi-reflectionless SIC-based BPF is shown in Fig. 6(a) and (b). It was characterized with a Keysight N5224A PNA and exhibits the following RF measured performance [see Fig. 7]: f_c tuning between 2.68-3.40 GHz (1.3:1), minimum in-band IL between 1.10-2.78 dB, 3-dB fractional BW (FBW) between 5.18%-6.76% and effective quality factor Q_{eff} = 180 at 3 GHz A comparison with one of its corresponding EM simulated states is shown in Fig. 7(a), which appears to be in a good agreement. Figs. 8

TABLE I
COMPARISON WITH STATE-OF-THE-ART REFLECTIONLESS BPFS

Ref.	Tech.	Sym	Freq.(GHz)	FBW(%)	IL (dB)	*#N*
[9]	LE	No	0.23-0.26	6.5-6.8	3.4-3.9	6
[10]	MS	No	2.11-2.72	5.9-7.6	1	3
[12]	MS	Yes	2.45	23.6	0.9	8
[13]	MS	Yes	2.45	6	2.2	5
[14]	MS	Yes	1.98	27	0.2	5
[11]	MMIC	Yes	2.7	29.6	3	6
TW	SIC	Yes	2.68-3.40	5.2-6.8	1.1-2.8	3
	SIC	Yes	2.60-3.35	4.2-5.4	3.1-3.7	5

(TW: This work, Tech.: Technology, MS: Microstrip, Ref: reference, Sym.: Symmetrical, *#N*: Number of resonators)

and 9(b) respectively demonstrate the two-stage prototype and its RF measured performance that can be summarized as follows: f_c tuning between 2.60-3.35 GHz, minimum in-band IL between 3.14-3.72 dB, 3-dB FBW between 4.23%-5.37% and $Q_{eff} = 150$ at 3 GHz. A comparison with one EM simulated state is also provided in Fig. 9(a), which exhibits a fair agreement between the simulation and measurement result, successfully validating the proposed SIC-resonator-based quasi-reflectionless BPF concept. It should be noticed that the S_{11} and S_{22} are not identical in the two-stage case due to the geometrical asymmetry (i.e., resistor location) in the shared bandstop section. Nevertheless, a quasi-reflectionless behavior is achieved at both ports. The discrepancy between the measured and simulated loss is due to manufacturing tolerances and assembly errors, as well as the surface roughness and loss of the Cu disks. A comparison of the proposed concept with state-of-the-art planar and lumped element reflectionless BPFs is provided in Table I. As shown, the proposed concept is the only symmetric quasi-reflectionless BPF that is based on a high-Q integration scheme using 3D SIC resonators. Furthermore, it exhibits lower IL and wider tuning range than its lumped element and planar counterparts in [9] and [13].

IV. CONCLUSION

This brief has presented the design, manufacturing, and testing of SIC resonator-based BPFs with symmetric quasi-reflectionless characteristics. Frequency agility and size compactness are obtained by tuning the capacitively-loaded SIC resonators with commercially-available linear actuators. Various EM design and integration aspects were discussed in detail. The operating principles of the proposed tunable quasi-reflectionless SIC-resonator-based BPF were experimentally validated at S-band through the manufacturing and testing of a one-stage and a two-stage prototypes.

REFERENCES

[1] R. M. Narayanan, K. A. Gallagher, G. J. Mazzaro, A. F. Martone, and K. D. Sherbondy, "Hardware design of a high dynamic range radio frequency (RF) harmonic measurement system," *Instruments*, vol. 2, no. 3, p. 16, 2018.

[2] A. Mishra and C. Li, "5.8-GHz ISM band intermodulation radar for high-sensitivity motion-sensing applications," in *Proc. IEEE Radio Wireless Symp.*, Anaheim, CA, USA, 2018, pp. 4–6.

[3] B. Mini-Circuits, "Reflectionless filters improve linearity and dynamic range," *Microw. J.*, vol. 58, no. 8, pp. 42–50, 2015.

[4] H. Dong, J. R. Smith, and J. L. Young, "A wide-band, high isolation UHF lumped-element ferrite circulator," *IEEE Microw. Wireless Compon. Lett.*, vol. 23, no. 6, pp. 294–296, Jun. 2013.

[5] N. A. Estep, D. L. Sounas, and A. Alù, "Magnetless microwave circulators based on spatiotemporally modulated rings of coupled resonators," *IEEE Trans. Microw. Theory Techn.*, vol. 64, no. 2, pp. 502–518, Feb. 2016.

[6] S. W. Y. Mung and W. S. Chan, "Active three-way circulator using transistor feedback network," *IEEE Microw. Wireless Compon. Lett.*, vol. 27, no. 5, pp. 476–478, May 2017.

[7] R. Gómez-García, J.-M. Muñoz-Ferreras, and D. Psychogiou, "RF reflectionless filtering power dividers," *IEEE Trans. Circuits Syst. II, Exp. Briefs*, vol. 66, no. 6, pp. 933–937, Jun. 2019.

[8] M. Kong, Y. Wu, Z. Zhuang, W. Wang, and C. Wang, "Ultra-miniaturized wideband input-absorptive bandstop filter based on TFIPD technology," *IEEE Trans. Circuits Syst. II, Exp. Briefs*, vol. 68, no. 7, pp. 2414–2418, Jul. 2021.

[9] D. Psychogiou and R. Gómez-García, "Reflectionless adaptive RF filters: Bandpass, bandstop, and cascade designs," *IEEE Trans. Microw. Theory Techn.*, vol. 65, no. 11, pp. 4593–4605, Nov. 2017.

[10] M. Fan, K. Song, L. Yang, and R. Gómez-García, "Frequency-reconfigurable input-reflectionless bandpass filter and filtering power divider with constant absolute bandwidth," *IEEE Trans. Circuits Syst. II, Exp. Briefs*, vol. 68, no. 7, pp. 2424–2428, Jul. 2021.

[11] M. A. Morgan and T. A. Boyd, "Reflectionless filter structures," *IEEE Trans. Microw. Theory Techn.*, vol. 63, no. 4, pp. 1263–1271, Apr. 2015.

[12] X. Wu, X. Liu, and Y. Li, "High-order dual-port quasi-absorptive microstrip coupled-line bandpass filters," *IEEE Trans. Microw. Theory Techn.*, vol. 68, no. 4, pp. 1462–1475, Apr. 2020.

[13] R. Gomez-Garcia, J.-M. Munoz-Ferreras, and D. Psychogiou, "Symmetrical quasi-absorptive RF bandpass filters," *IEEE Trans. Microw. Theory Techn.*, vol. 67, no. 4, pp. 1472–1482, Apr. 2019.

[14] C. Luo *et al.*, "Quasi-reflectionless microstrip bandpass filters using bandstop filter for out-of-band improvement," *IEEE Trans. Circuits Syst. II, Exp. Briefs*, vol. 67, no. 10, pp. 1849–1853, Oct. 2020.

[15] L. Yang, R. Gómez-García, J. Muñoz-Ferreras, R. Zhang, and D. Peroulis, "Reflectionless wideband bandpass filter designed with multilayered microstrip vertical transition," in *Proc. IEEE MTT-S Int. Wireless Symp.*, Guangzhou, China, 2019, pp. 1–3.

[16] H.-W. Xie, K. Zhou, C.-X. Zhou, and W. Wu, "Compact SIW diplexers and dual-band bandpass filter with wide-stopband performances," *IEEE Trans.Circuits Syst. II, Exp. Briefs*, vol. 67, no. 12, pp. 2933–2937, Dec. 2020

[17] H.-W. Xie, K. Zhou, C.-X. Zhou, and W. Wu, "Wide-stopband SIW filters using modified multi-spurious modes suppression technique," *IEEE Trans.Circuits Syst. II, Exp. Briefs*, vol. 67, no. 12, pp. 2883–2887, Dec. 2020.

[18] J. D. Martinez, S. Sirci, V. E. Boria, and M. A. Sanchez-Soriano, "When compactness meets flexibility: Basic coaxial SIW filter topology for device miniaturization, design flexibility, advanced filtering responses, and implementation of tunable filters," *IEEE Microw. Mag.*, vol. 21, no. 6, pp. 58–78, Jun. 2020.

[19] A. Anand and X. Liu, "Reconfigurable planar capacitive coupling in substrate-integrated coaxial-cavity filters," *IEEE Trans. Microw. Theory Techn.*, vol. 64, no. 8, pp. 2548–2560, Aug. 2016.

[20] I. S. Krishna and S. Mukherjee, "Triple-mode substrate integrated coaxial resonator based bandpass filter featuring flexible transmission zeros and adjustable bandwidth," *IEEE Trans. Circuits Syst. II, Exp. Briefs*, vol. 68, no. 4, pp. 1223–1227, Apr. 2021.

[21] M. Abdelfattah and D. Peroulis, "High-Q tunable evanescent-mode cavity SIW resonators and filters with contactless tuners," *IEEE Trans. Microw. Theory Techn.*, vol. 67, no. 9, pp. 3661–3672, Sep. 2019.

[22] A. Anand and X. Liu, "Capacitively tuned electrical coupling for reconfigurable coaxial cavity bandstop filters," in *Proc. IEEE MTT-S Int. Microw. Symp.*, Phoenix, AZ, USA, 2015, pp. 1–3.

[23] D. Psychogiou and R. Gómez-García, "Compact substrate-integrated bandstop filters using double-resonant coaxial resonators," *IEEE Microw. Wireless Compon. Lett.*, vol. 30, no. 10, pp. 941–944, Oct. 2020.

[24] D. Psychogiou, B. Vaughn, R. Gómez-García, and D. Peroulis, "Reconfigurable multiband bandpass filters in evanescent-mode-cavity-resonator technology," *IEEE Microw. Wireless Compon. Lett.*, vol. 27, no. 3, pp. 248–250, Mar. 2017.

[25] New Scale Technologies. (2018). *M3-L Micro Linear Actuator With Embedded Controller*. [Online]. Available: https://www.newscaletech.com/micro-motion-modules/m3-l-linear-smart-actuators